




Article

New Insights into the Mechanism of Antibacterial Action of Synthetic Peptide *Mo-CBP₃-PepI* against *Klebsiella pneumoniae*

Levi A. C. Branco ^{1,†}, Pedro F. N. Souza ^{1,2,*,†} , Nilton A. S. Neto ¹, Tawanny K. B. Aguiar ¹ , Ayrles F. B. Silva ¹, Rômulo F. Carneiro ³, Celso S. Nagano ³, Felipe P. Mesquita ², Luina B. Lima ² and Cleverson D. T. Freitas ¹ 

¹ Department of Biochemistry and Molecular Biology, Federal University of Ceará, Fortaleza 60020-181, CE, Brazil

² Drug Research and Development Center, Department of Physiology and Pharmacology, Federal University of Ceará, Fortaleza 60020-181, CE, Brazil

³ Department of Fisheries Engineering, Federal University of Ceará, Fortaleza 60020-181, CE, Brazil

* Correspondence: pedrofilhobio@gmail.com or pedrofilhobio@ufc.br

† These authors contributed equally to this work.

Abstract: *Klebsiella pneumoniae* is a multidrug-resistant opportunistic human pathogen related to various infections. As such, synthetic peptides have emerged as potential alternative molecules. *Mo-CBP₃-PepI* has presented great activity against *K. pneumoniae* by presenting an MIC₅₀ at a very low concentration (31.25 µg mL⁻¹). Here, fluorescence microscopy and proteomic analysis revealed the alteration in cell membrane permeability, ROS overproduction, and protein profile of *K. pneumoniae* cells treated with *Mo-CBP₃-PepI*. *Mo-CBP₃-PepI* led to ROS overaccumulation and membrane pore formation in *K. pneumoniae* cells. Furthermore, the proteomic analysis highlighted changes in essential metabolic pathways. For example, after treatment of *K. pneumoniae* cells with *Mo-CBP₃-PepI*, a reduction in the abundance of protein related to DNA and protein metabolism, cytoskeleton and cell wall organization, redox metabolism, regulation factors, ribosomal proteins, and resistance to antibiotics was seen. The reduction in proteins involved in vital processes for cell life, such as DNA repair, cell wall turnover, and protein turnover, results in the accumulation of ROS, driving the cell to death. Our findings indicated that *Mo-CBP₃-PepI* might have mechanisms of action against *K. pneumoniae* cells, mitigating the development of resistance and thus being a potent molecule to be employed in producing new drugs against *K. pneumoniae* infections.

Keywords: multidrug-resistant bacteria; proteomic analysis; synthetic peptides; antibacterial peptides



Citation: Branco, L.A.C.; Souza, P.F.N.; Neto, N.A.S.; Aguiar, T.K.B.; Silva, A.F.B.; Carneiro, R.F.; Nagano, C.S.; Mesquita, F.P.; Lima, L.B.; Freitas, C.D.T. New Insights into the Mechanism of Antibacterial Action of Synthetic Peptide *Mo-CBP₃-PepI* against *Klebsiella pneumoniae*. *Antibiotics* **2022**, *11*, 1753. <https://doi.org/10.3390/antibiotics11121753>

Academic Editor: Maria Fernanda N. N. Carvalho

Received: 14 November 2022

Accepted: 1 December 2022

Published: 4 December 2022

Publisher's Note: MDPI stays neutral with regard to jurisdictional claims in published maps and institutional affiliations.



Copyright: © 2022 by the authors. Licensee MDPI, Basel, Switzerland. This article is an open access article distributed under the terms and conditions of the Creative Commons Attribution (CC BY) license (<https://creativecommons.org/licenses/by/4.0/>).

1. Introduction

The emergence of multidrug-resistant bacteria (MDRB) is a challenge to public health worldwide, leading to lengthy hospital stays, high healthcare costs around USD 1 million, and a death rate of 46.31% [1–3]. *K. pneumoniae* is a Gram-negative bacterium that colonizes the human gastrointestinal system and often is found in feces [4]. Additionally, *K. pneumoniae* is a bacterium belonging to the ESKAPE (*Enterococcus faecium*, *Staphylococcus aureus*, *Klebsiella pneumoniae*, *Acinetobacter baumannii*, *Pseudomonas aeruginosa*, and *Enterobacter* species) group of MDRB that are pathogenic to humans [5,6].

K. pneumoniae is an opportunistic MDRB only able to infect people with a compromised immune system [4]. *K. pneumoniae* presents resistance against polymyxins, carbapenems, fluoroquinolones, aminoglycosides, tetracyclines, third-generation cephalosporins, and is pan drug-resistant [7–9]. The clinical manifestations of *K. pneumoniae* present as an acute bacterial skin infection, bacteremia, pneumonia, and osteoarticular infection [10–12].

The multidrug resistance acquired by *K. pneumoniae* made this bacterium an important pathogen threatening human health. Based on that, it is emergent and imperative to seek new molecules to fight back in two ways: (1) to develop a new drug to produce a new treatment; or (2) to produce a new molecule that could act synergistically with commercial

drugs making them effective again [1]. In this scenario, antimicrobial peptides represent a notorious group of molecules that could help scientists quickly find a way to cope with antimicrobial resistance [13]. However, natural antimicrobial peptides have presented problems in clinical trials, such as toxicity to host cells, low resistance to proteolysis, and sometimes high cost of obtention [13,14].

Synthetic antimicrobial peptides emerged as a solution to solve the problems presented by natural antimicrobial peptides. Synthetic antimicrobial peptides are designed using a natural model sequence to have higher antimicrobial activity, greater resistance to proteolysis, and no toxicity to host cells. Recently, our research group has designed synthetic peptides called *Mo*-CBP₃-PepI using the sequence of a chitin-binding protein from *Moringa oleifera* [15]. *Mo*-CBP₃-PepI is a non-hemolytic small cationic peptide with a net charge +1, a molecular mass of 893.10 Da, and a hydrophobic ratio of 62%. It has a secondary structure as α -helix confirmed by circular dichroism assays [15].

Regarding the antimicrobial potential, *Mo*-CBP₃-PepI presents great anticandidal activity against *Candida albicans*, *C. parapsilosis*, *C. krusei*, and *C. tropicalis*. The mechanisms of action of *Mo*-CBP₃-PepI against the *Candida* genus were revealed using *C. albicans* as a model [15–17]. Regarding the antibacterial activity, *Mo*-CBP₃-PepI, the only relevant activity, was evaluated against *K. pneumoniae*. Therefore, this study employed fluorescence and scanning electron microscopes and proteomic analysis to provide new insights into the mechanism of antibacterial action of *Mo*-CBP₃-PepI against *K. pneumoniae*. Additionally, toxicity tests were performed against human cells to produce new data on the safety of *Mo*-CBP₃-PepI.

2. Material and Methods

2.1. Biological Material

The human-pathogenic Gram-negative bacteria *K. pneumoniae* (ATCC 10031) strain was obtained from the Laboratory of Plant Toxins (LABTOX) of the Federal University of Ceará (UFC).

2.2. Peptide Synthesis

The synthetic peptide *Mo*-CBP₃-PepI (CPAIQRCC) [15] was chemically synthesized by the company ChemPeptide (Shanghai, China), where its purity and quality of it were tested by mass spectrometry and reverse-phase high-performance liquid chromatography (Figure S1 (Supplementary Materials)).

2.3. Cell Viability by MTT Assay

The cell viability assay was performed as described by Lima et al. [17], with some adjustments. After the antibacterial assay was completed as described by Oliveira et al. [15], the wells containing the treated cells with *Mo*-CBP₃-PepI at 1 mg mL⁻¹ and control cells (50 μ L) were incubated for 3 h in the dark at 37 °C with 50 μ L of 3-(4,5-dimethylthiazol-2-yl)-2,5-diphenyltetrazolium bromide (2 mg mL⁻¹, MTT). After incubation, 100 μ L of 100% DMSO was added to the wells, and the plate was slowly shaken to dissolve the formazan crystals. The absorbance was measured using a microplate reader (Epoch, BioTek) with a wavelength of 495 nm. The controls used for this assay were 5% of dimethyl sulfoxide (DMSO) prepared in 0.15 M NaCl (saline) solution and ciprofloxacin (1000 μ g mL⁻¹) prepared in 5% ethanol in sterile saline solution.

2.4. Antibiofilm Assay

The antibiofilm assay was conducted in flat-bottom 96-well polystyrene microplates as described by Neto et al. [18]. A single colony of *K. pneumoniae* was collected in stock Petri plates containing inoculated Mueller–Hinton agar. The colony was used as inoculum for 5 mL of Mueller–Hinton broth, and the media was incubated for 24 h in the dark at 37 °C. In sequence, the O.D. of the cell suspension was measured using a microplate reader (Epoch, BioTek) and adjusted to 0.1 at 630 nm with Mueller–Hinton broth. For the inhibition of

biofilm formation, 50 μL of the cell (2.5×10^{-5} CFU mL^{-1}) suspension was incubated with 50 μL of the peptide ($31.25 \mu\text{g mL}^{-1}$) solution and 50 μL of the respective controls described above. The incubation lasted for 48 h at 37 °C. For the biofilm degradation assay, 50 μL of the cell suspension was incubated for 24 h at 37 °C. After this, 50 μL of the peptide solution and the respective controls were added to the wells containing the preformed biofilm and incubated for 24 h at 37 °C.

After incubation, both wells of biofilm formation inhibition and biofilm degradation were washed once with a sterile saline solution. Then, the wells were fixated with 100 μL methanol 99% for 15 min. After the methanol was removed and the plates were dried at 37 °C, then, the wells were stained with 200 μL of 0.1% violet crystal solution for 20 min. In sequence, the wells were washed three times with distilled water. Then, the crystals stained on the biofilm were diluted with 200 μL of 33% acetic acid, and the O.D was measured using a wavelength of 600 nm. The assay was executed in triplicate, with three independent biological experiments.

2.5. Mechanism of Action Evaluation by Fluorescence Microscopy

2.5.1. Cell Membrane Integrity by Propidium Iodide (PI) and FITC-Dextran Uptake

The assay was conducted as described by Oliveira et al. [15], with some modifications. Preparation of cell suspension was completed as mentioned above. After, 50 μL of the diluted bacteria solution was incubated in the dark for 24 h, at 37 °C, with 50 μL of the peptide solution ($31.25 \mu\text{g mL}^{-1}$) previously prepared with 5% of dimethyl sulfoxide (DMSO) diluted in 0.15 M NaCl solution. The assay was conducted in 1.5 mL microtubes. The diluted bacteria solution was incubated only with the DMSO-NaCl solution for control. After incubation, the microtubes were centrifuged ($5000 \times g$, 5 min, 4 °C) and washed three times. Next, the washed cells were incubated with 1 μM propidium iodide for 30 min, in the dark, at 37 °C. After this, the cells were washed two times with saline solution to remove the excess fluorophore and observed with a fluorescence microscope (Olympus System BX 60; excitation wavelength, 488 nm; emission wavelength, 525 nm).

Additionally, to know the size of the pore formed, in a new experiment completed precisely as above, cells were incubated with FITC-Dextran (fluorescein isothiocyanate (FITC)-Dextran) with a size of 10-kDa. After incubation for 30 min, cells were washed with 0.15 M of NaCl and visualized in light and fluorescence microscope Olympus System BX 60 with an excitation wavelength of 490 nm and emission wavelength of 520 nm.

2.5.2. Detection of Peptide-Induced Overproduction of Reactive Oxygen Species (ROS)

This assay was conducted in the same way as above but with a few differences. The preparation of cell suspension and the antimicrobial assay was performed in the same way described above. After the three rounds of centrifugation and washes, the cells were incubated with 1 mM 2,7-dichlorofluorescein diacetate (DCFH-DA) [19] for 30 min, in the dark, at 37 °C. After the washes, the cells were also observed under a fluorescence microscope (Olympus System BX60; excitation wavelength, 488 nm; emission wavelength, 525 nm).

2.5.3. Scanning Electronic Microscopy (SEM) Analysis

SEM analysis was conducted as described by Staniszevska et al. [20]. After the antibacterial assay, cells were centrifuged ($5000 \times g$, 5 min, 4 °C), the supernatant was removed, cells resuspended, and fixated for 5 h in a fixation solution (2.5% glutaraldehyde (*v/v*) in 0.15 M Na-phosphate buffer, pH: 7.2). After centrifugations as described above, the cells were washed three times with 0.15 M Na-phosphate buffer, pH: 7.2. For dehydration, the samples were incubated and dried with ethanol (30%, 50%, 70%, 100%, 100% (*v/v*)) for 10 min each, and centrifugation as described above after each incubation time. Lastly, the samples were incubated with 50/50 ethanol/hexamethyldisilane (HMDS) for 10 min and centrifuged. Then, the pellet was washed with 100% HMDS and transferred to a coverslip to dry out. After complete drying, the coverslips were assembled on stubs and coated

with a 20 nm gold layer using a PET coating machine (EMITECH—Q150TES; Quorum Technologies, Lewes, England). The SEM analyses were completed with an InSpec™ 50 FEI Scanning Electron Microscope, equipped with a low energy detector (Everhart Thornley detector), using an acceleration beam voltage of 20,000 kV and 20,000× detector magnification.

2.6. Protein Extraction and Gel-Free Proteomic Analysis

Initially, an antibacterial assay was performed within 24 h of incubation, using the best inhibitory concentration of *Mo*-CBP₃-PepI (31.25 µg mL⁻¹) [15]. After this, samples were washed twice with 50 mM sodium acetate pH 5.2, with centrifugations at 12,000× *g* for 15 min at 4 °C. At the end of the washes, the samples were resuspended in 300 µL in the same buffer and frozen for 24 h. Then, the frozen samples were sonicated for 30 min to break the cell wall and membrane, the samples were centrifuged again, and the supernatant was collected.

After that, the Bradford assay was performed to determine the protein concentration in the samples. This step was followed by adding a 10 mM DTT solution under incubation for 1 h at 37 °C to reduce the proteins. Then iodoacetamide was added to a final concentration of 15 mM and incubated for 30 min in a dark room to alkylate the reduced proteins. The proteins reduced and alkylated were digested using trypsin gold (Promega, Madison, WI, USA) to a final concentration of 1:20 (*w/w*) as described by manufacturers. The trypsin digestion was performed for 16 h at 37 °C. Finally, the samples were dried in a speed vacuum (Eppendorf, Hamburg, Germany) for 3 h and analyzed by ESI-QUAD-TOF mass spectrometer.

2.7. Protein Identification

Tandem mass spectra were extracted into PKL files for both samples, and the proteins were searched using MASCOT MS/MS ions search from MATRIX SCIENCE (https://www.matrixscience.com/cgi/search_form.pl?FORMVER=2&SEARCH=MIS (accessed on 15 September 2022)) against UP625_E_coli_K12 (AA), UP808_K_pneumoniae and SwissProt databases (the taxonomy was set in bacteria). The terms for the search were: fixed modifications to Carbamidomethyl (C); variable modifications to Oxidation (O); the Peptide tolerance was set to 1.2 DA (with 1% FDR); the MS/MS tolerance was set to 0.6 DA; the peptide charge was set to 2+, 3+, and 4+; and finally, the instrument was set to ESI-QUAD-TOF. The proteins identified in both samples were searched for in UNIPROT and separated into 3 sets (unique from control, unique from the cells treated with *Mo*-CBP₃-PepI, and *Mo*-CBP₃-PepI x control shared proteins).

The proteins with a fold-change value ≥ 1.5 ($p < 0.05$, Tukey's test) that were up-accumulated (increased the abundance), and proteins with a fold-change value ≤ 0.5 ($p < 0.05$, Tukey's test) that were down-accumulated (decreased the abundance) were taken into consideration for comparisons. For each protein, its corresponding FASTA file was downloaded. Then, the blast2go program (<https://www.blast2go.com/> (accessed on 30 September 2022)) was used to categorize the proteins detected by Gene Ontology (GO) annotation according to Molecular function, Biological Activity, and subcellular location.

2.8. Cytotoxicity Assay

The cytotoxicity assay was assessed by measuring the ability of live cells to convert a yellow dye, 3-(4,5-dimethyl-2-thiazolyl)-2,5-diphenyl-2H-tetrazolium bromide (MTT), to formazan. The cell lines used were L929 (murine fibroblasts, ATCC number CCL-1), MRC-5 (human lung fibroblasts, ATCC number CCL-171), and HaCaT (human keratinocytes) following the methodology described by Souza et al. [14]. Cells were treated with *Mo*-CBP₃-PepI at 1 mg mL⁻¹. The alkylating agent methyl methanesulfonate (MMS) at 4×10^{-5} M was used as the positive control. The MTT formazan product was dissolved in 150 µL of DMSO, and the absorbance was measured using a multiplate reader (Spectra Count,

Packard, Mississauga, ON, Canada). The drug effect was quantified as the percentage of control absorbance of the reduced dye at 595 nm.

2.9. Comet Assay

For this assay, MMS at 4×10^{-5} M was used as the positive control for DNA damage, and peptides were assayed at 1 mg mL^{-1} . The standard alkaline comet assay (single-cell gel electrophoresis) after treatment (24 h). Cells were washed with ice-cold PBS, trypsinized, and resuspended in a complete medium. Thus, $20 \mu\text{L}$ of cell suspension (0.7×10^5 cells/mL) was dissolved in 0.75% low-melting-point agarose. Slides were incubated in ice-cold lysis solution (2.5 M NaCl, 0.01 M Tris, 0.1 M EDTA, 1% Triton X-100, and 10% DMSO, pH 10.0) at 4°C for at least 1 h to remove cell membranes, leaving DNA as “nucleoids”. Afterward, the slides were placed in a horizontal electrophoresis unit and incubated with fresh buffer solution (0.3 M NaOH, 0.001 M EDTA, pH 13.0) at 4°C for 20 min to allow DNA to unwind and the expression of alkali-labile sites. Electrophoresis was conducted for 20 min at 25 V (94 V/cm). All the above steps were performed in the dark to prevent additional DNA damage. Slides were neutralized (0.4 M Tris, pH 7.5) and stained using $20 \mu\text{g mL}^{-1}$ of ethidium bromide. Three hundred cells (100 cells from each of the three replicate slides for each treatment) were selected, coded, and blindly analyzed for DNA migration. These cells were visually scored according to tail length into five classes:

Class 0: undamaged, without a tail;

Class 1: with a tail shorter than the diameter of the head nucleus;

Class 2: with tail length 1–2× the diameter of the head;

Class 3: with a tail longer than 2× the diameter of the head;

Class 4: comets with no heads.

The index of damage (ID) value was calculated for each sample. The ID was defined as an arbitrary score based on the number of cells in the different damage classes, which are visually scored by measuring DNA migration length and the amount of DNA in the tail. DI ranges from 0 (no tail: $100 \text{ cells} \times 0$) to 400 (with maximum migration: $100 \text{ cells} \times 4$).

2.10. Morphological Analysis of Apoptotic Cells

For this assay, the concentration of peptides was 1 mg mL^{-1} . DMSO-NaCl was the negative control for damage, and MMS at 4×10^{-5} M was used as the positive control for DNA damage. Peptides and control solutions were incubated as described above. Cells with the morphological characteristics of apoptosis, such as apoptotic bodies, peripheral condensation of chromatin, fragmented nucleus, and small cell volume, were evaluated after 24 h of treatment, either with controls or peptides. The evaluation was executed using acridine orange (AO)/ethidium bromide (EB) staining assay. A total of $50 \mu\text{L}$ of the cell suspension was mixed with $1 \mu\text{L}$ of the staining solution ($100 \mu\text{g/mL}$ AO + $100 \mu\text{g/mL}$ EB in PBS) and spread on a slide, where 300 cells were counted per data point.

3. Results and Discussion

3.1. Cell Viability and Antibiofilm Activity of Mo-CBP₃-PepI against *K. pneumoniae*

As reported in a previous work by Oliveira et al. [15], Mo-CBP₃-PepI presented an MIC₅₀ against *K. pneumoniae* at $31.25 \mu\text{g mL}^{-1}$. The experiments we repeated here led to the same results, corroborating the data presented by Oliveira et al. [15]. The concentration of Mo-CBP₃-PepI to reach an MIC₅₀ against *K. pneumoniae* is very low compared to other synthetic peptides [21,22]. For example, Fleeman et al. [21] showed that the synthetic peptide called PepC, which presented an MIC₅₀ at a concentration of $350 \mu\text{g mL}^{-1}$ 11 times higher than the concentration presented by Mo-CBP₃-PepI. Additionally, Tincho et al. [22] tested three synthetic peptides, and all presented an MIC₅₀ against *K. pneumoniae* at a concentration of $500 \mu\text{g mL}^{-1}$, 16.07 times higher than Mo-CBP₃-PepI. These results revealed that Mo-CBP₃-PepI is much more effective against *K. pneumoniae* than other synthetic peptides.

We further evaluated the cell viability of *K. pneumoniae* cells and biofilm formation after treatment with Mo-CBP₃-PepI. The first was to evaluate the number of viable cells after

treatment with *Mo*-CBP₃-PepI (Table 1). The MTT assay revealed that only 47.54% ± 0.008 of *K. pneumoniae* cells were viable after incubation with *Mo*-CBP₃-PepI, which agrees with the data of MIC₅₀. These results prove that *Mo*-CBP₃-PepI kills half of the cells at the tested concentration. Otherwise, 100% of *K. pneumoniae* cells were viable in control treated with 5% DMSO in 0.15 M NaCl (Table 1).

Table 1. Cell viability and antibiofilm potential of *Mo*-CBP₃-PepI against *K. pneumoniae*.

Treatments	^a MIC ₅₀ of <i>Mo</i> -CBP ₃ -PepI toward <i>K. pneumoniae</i> Antibiofilm Potential		
	Cell Viability (%)	Inhibition of Biofilm Formation (%)	Degradation of Preformed Biofilm (%)
DMSO	100 ± 0.005	0	0
<i>Mo</i> -CBP ₃ -PepI	47.54 ± 0.008	11.87 ± 0.001	0

^a The MIC₅₀ concentration was 31.25 µg mL⁻¹, as defined by Oliveira et al. [1]. Cell viability assay was executed with planktonic cells.

Moving forward, the antibiofilm potential of *Mo*-CBP₃-PepI toward *K. pneumoniae* was evaluated. *Mo*-CBP₃-PepI barely inhibited the biofilm formation of *K. pneumoniae*, only 11.87% ± 0.001, and presented no activity against the preformed biofilm (Table 1). As expected, the control solution was ineffective in inhibiting the formation or degrading the preformed biofilms of *K. pneumoniae* (Table 1).

3.2. Toxicity of *Mo*-CBP₃-PepI to Human Cells

Before we move forward with the study to understand the mechanisms of action of *Mo*-CBP₃-PepI against *K. pneumoniae*, toxicity tests against human cells were needed to provide information that might indicate the application of *Mo*-CBP₃-PepI. For example, Oliveira et al. [15] presented a safe *Mo*-CBP₃-PepI based on the absence of hemolytic activity against human red blood cells even at concentrations (120 µg mL⁻¹) four times higher than MIC₅₀ concentration [15].

In this study, we went further in the analysis of toxicity. *Mo*-CBP₃-PepI was assayed against other human cells (Figure 1). MTT assay and morphological analysis of human fetal lung fibroblast (MRC-5 line), human keratinocytes (HaCaT line), and L929 fibroblast cells from mice revealed that *Mo*-CBP₃-PepI did not affect either cell viability and morphology of those cells even at a concentration of 1 mg mL⁻¹, which is 32 times higher than MIC₅₀ concentration. In contrast, the positive control for damage methyl methanesulfonate (MMS) (4 × 10⁻⁵ M) led to the death of all cells. It caused severe damage to DNA and nuclei structure indicating the establishment of cell death (Figure 1).

Another experiment to evaluate damage and fragmentation of DNA caused by *Mo*-CBP₃-PepI was evaluated by Comet assay (Figure 2) against the same cell lines and at the same concentration. The assay revealed that the DNA of cells treated with peptides presented no damage. In contrast, cells treated with MMS presented with completely damaged DNA (Figure 2). These results assure that the peptide is either safe or presents a low risk for human cells. Other peptides have presented high toxicity to human red blood cells and other human-type cells, such as WRL-68 (liver cells) and NL-20 (lung cells) [23].

The synthetic peptides RN7-IN10, RN7-IN9, RN7-IN8, RN7-IN7, and RN7-IN6, derived from indolicidin and ranalexin, presented 50% of hemolytic activity, respectively, at 62.5, 62.5, 125, and 125 µg mL⁻¹ [23]. Additionally, the authors revealed that the synthetic peptides RN7-IN10, RN7-IN9, RN7-IN8, RN7-IN7, and RN7-IN6 were toxic to human cell lines such as WRL-68 (liver cells) and NL-20 (lung cells) at a concentration of 125 µg mL⁻¹ [23]. These concentrations show that those peptides are more toxic than *Mo*-CBP₃-PepI. Therefore, based on the results of the toxicity of *Mo*-CBP₃-PepI, we decided to move forward in the experiment of the mechanism of action.

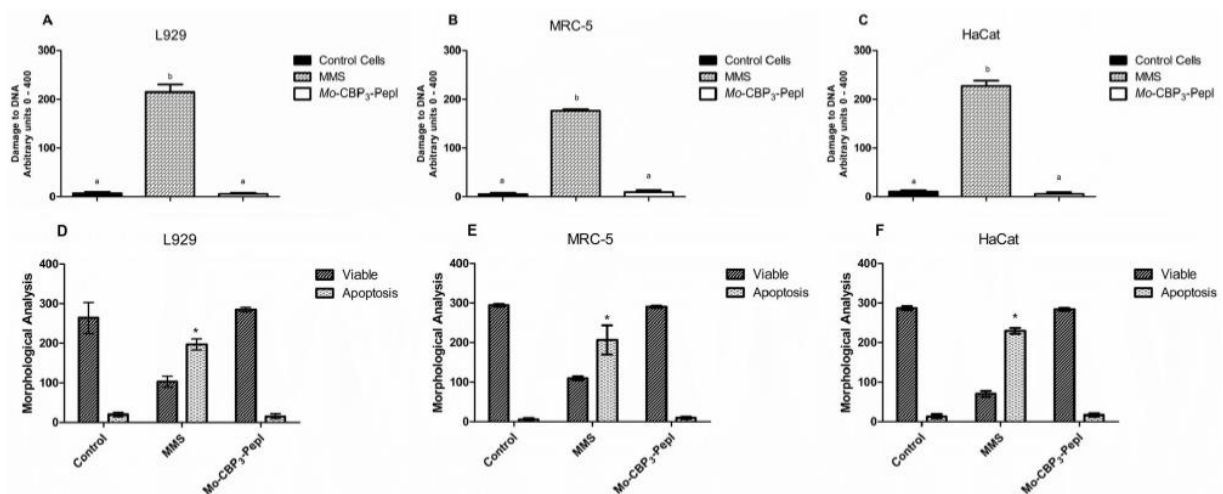


Figure 1. Assessment of toxicity of *Mo-CBP₃-PepI* to human cell lines. (A) L929, (B) HaCaT, and (C) MRC-5 lines were incubated with synthetic peptide at a concentration of 1 mg mL^{-1} to evaluate the damage to DNA by comet assay. (D–F) Cell lines were incubated with peptides as described and evaluated for viable cells and cells in apoptosis. MMS ($4 \times 10^{-5} \text{ M}$) was employed as a positive control for cell toxicity, and healthy cells as a negative control for toxicity. Data are shown as mean \pm standard deviation of three independent experiments. * $p < 0.05$. Small letters indicate statistical significance.

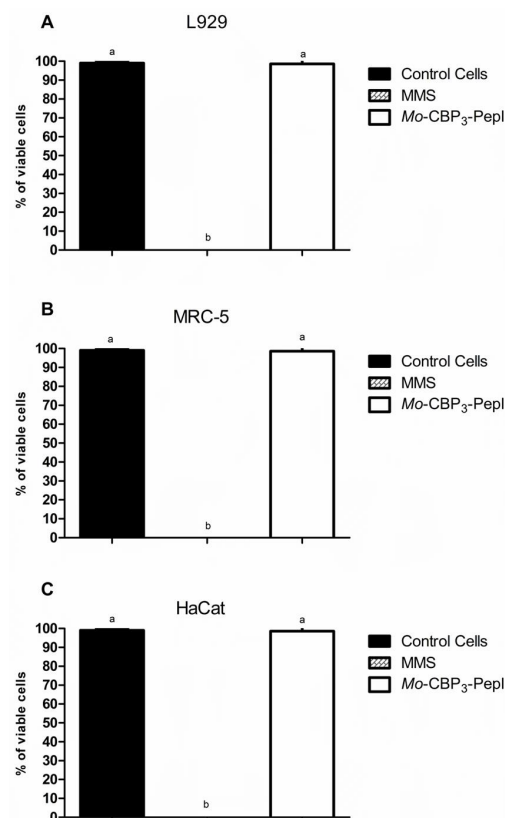


Figure 2. Evaluation of toxicity of *Mo-CBP₃-PepI* to human cell lines by MTT viability assay. In (A) L929, (B) HaCaT, and (C) MRC-5 lines were incubated with synthetic peptides at a concentration of 1 mg mL^{-1} . Methyl methanesulfonate (MMS; $4 \times 10^{-5} \text{ M}$) was employed as a positive control for cell toxicity, and healthy cells as a negative control for toxicity. Data are shown as mean \pm standard deviation of three independent experiments with significance of $p < 0.05$. Small letters indicate statistical significance.

3.3. Mechanism of Action of *Mo*-CBP₃-PepI against *K. pneumoniae*

3.3.1. Membrane Pore Formation and ROS Overproduction

The mechanisms employed by *Mo*-CBP₃-PepI against *K. pneumoniae* were evaluated against planktonic lifestyle, given that the biofilm activity was not satisfactory (Table 1). The assay to evaluate the pore in the membrane by PI uptake revealed that the treatment with *Mo*-CBP₃-PepI induced the pore formation in the membrane of *K. pneumoniae* cells, as revealed by the detected red fluorescence (Figure 3A,B,E,F). The green fluorescence of Dextran-FITC (Figure 3C,D,G,H) indicated that the pore formed by *Mo*-CBP₃-PepI in the membrane of *K. pneumoniae* cells is at least 10 kDa because the size fluorophore used is 10 kDa.

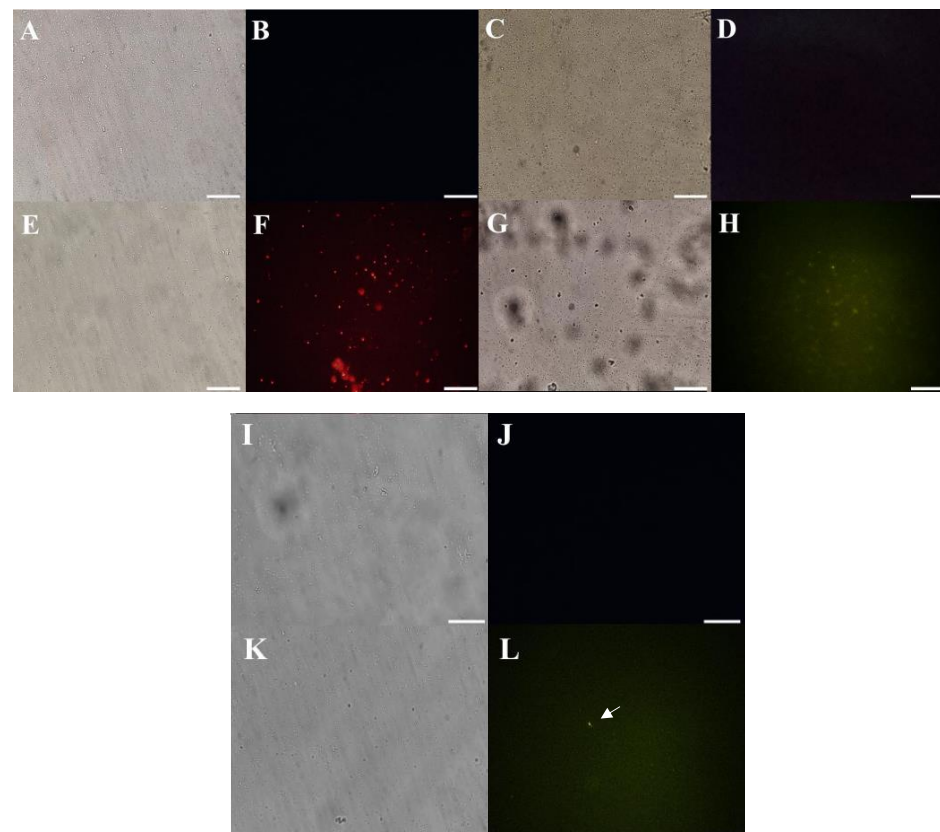


Figure 3. Mechanism of action of *Mo*-CBP₃-PepI assessed by fluorescence microscopy. In all experiments, *Mo*-CBP₃-PepI was used at a concentration of 31.26 $\mu\text{g mL}^{-1}$. (A,B) control *K. pneumoniae* cells for PI uptake assay. (E,F) *Mo*-CBP₃-PepI-treated *K. pneumoniae* cells for PI uptake assay. Red fluorescence (F) indicates pore formation induced by *Mo*-CBP₃-PepI. (C,D) control *K. pneumoniae* cells for FITC-Dextran uptake assay. (G,H) *Mo*-CBP₃-PepI-treated *K. pneumoniae* cells for FITC-Dextran uptake assay. Green fluorescence (H) indicates 10-kDa -sized pore formation induced by *Mo*-CBP₃-PepI. (I,J) control *K. pneumoniae* cells for ROS overproduction assay. (K,L) *Mo*-CBP₃-PepI-treated *K. pneumoniae* cells for ROS overproduction assay. Green fluorescence (L) indicates pore formation induced by *Mo*-CBP₃-PepI. Bars indicate 100 μm .

Membranes are the main target of synthetic or natural peptides [16,24]. This is different from antibiotics, which generally affect a protein leading to the rapid development of resistance. By targeting the membrane of *K. pneumoniae*, *Mo*-CBP₃-PepI imposes a challenging problem for cells to overcome. Membranes are a complex structure, highly conserved during cell evolution. So, remodeling plasma membrane upon external stress is metabolically expensive and dangerous to cells [14].

Mo-CBP₃-PepI, *Mo*-CBP₃-PepII, and *Mo*-CBP₃-PepIII are synthetic peptides derived from a chitin-binding protein purified from *Moringa oleifera* [15]. In the same way as

Mo-CBP3-PepII and Mo-CBP3-PepIII, Mo-CBP3-PepI can interact with chitin and induce membrane pores in important human pathogenic fungi such as *Candida* spp., *Cryptococcus neoformans*, and *Trichophyton mentagrophytes* [16,17,25]. Here, the mechanisms of action behind the antibacterial activity of Mo-CBP3-PepI against *K. pneumoniae* cells were evaluated. The movement of PI (Figure 3A,B,E,F) through the membrane of *K. pneumoniae* revealed by red fluorescence indicates the permeabilization by establishing a pore size of 692.50 Da [26,27]. The size is estimated to be 10 kDa (Figure 3C,D,G,H), given the green fluorescence released by Dextran-FITC.

The questions are, how does Mo-CBP₃-PepI induce pore formation in the membrane of *K. pneumoniae* cells, and why is the pore so big? To answer the first question, it is necessary to revert to the design process of Mo-CBP₃-PepI. During the design process, the Mo-CBP₃-PepI sequence was achieved for reaching three essential features for antimicrobial activity, positive net charge (+1), hydrophobic potential (62%), and probability of 100% to produce a secondary structure in α -helix [13,15,28]. First, the positive net charge of Mo-CBP₃-PepI given by the presence of an arginine residue is essential for the ionic attraction of Mo-CBP₃-PepI to negatively charged peptides in the outlier of *K. pneumoniae* membrane and initial insertion on it [29]. Second, the hydrophobic potential critical for interaction with the hydrophobic core of the membrane's lipid bilayer is conferred by the presence of apolar amino-acid residues [30]. Third, a secondary structure in α -helix is essential to the attraction and insertion of Mo-CBP₃-PepI into the *K. pneumoniae* [28]. Bioinformatics analysis revealed that Mo-CBP₃-PepI is a cell-penetrating peptide [15]. It is important to notice that *K. pneumoniae* is a Gram-negative bacterium with an outer membrane completely exposed to the Mo-CBP₃-PepI attack by the above mechanism.

To answer the second question, it is necessary to understand an essential characteristic of antimicrobial peptides, self-association [31]. Self-association is the ability of antimicrobial peptides to interact during the insertion into the membrane, allowing the formation of a huge pore [31]. Based on this result, it is hypothesized the establishment of a barrel-stave model induces pore formation. In this model, a peptide interacts with lipids in the membrane, as described above, to perform the insertion into the membrane. Then, the peptide molecules interact between them to form a huge pore on the membrane [31–33]. Lima et al. [16] showed that Mo-CBP₃-PepI induces the formation of a pore of 10 kDa in *C. albicans* cells.

In the same way, the evaluation of ROS overproduction in *K. pneumoniae* cells was evaluated. The treatment of *K. pneumoniae* cells with Mo-CBP₃-PepI led to a slight accumulation of ROS within cells. In contrast, control cells treated with DMSO did not present any ROS production, which was an expected result (Figure 3I,J). ROS are essential to cell development. However, the levels of ROS in the cell have to be regulated because higher accumulation than necessary could be lethal for the cell. The induction of overproduction of ROS could be lethal to cells (Figure 3K,L). The undesired and uncontrolled ROS production and accumulation are associated with damage in important cell life molecules such as proteins, lipids, and DNA, driving cells to death [26]. It is known that Mo-CBP₃-PepI can induce ROS overproduction in *C. albicans* cells [16]. However, the ability to induce ROS in bacterial cells is revealed for the first time. Rowe-Magnus et al. [34] showed that synthetic Cathelicidin-derived peptides induced ROS overproduction in the Gram-negative *Vibrio cholera*. The authors discuss that induction of ROS accumulation was mediated by damage caused in the membrane. Here, we showed that Mo-CBP₃-PepI could also induce pore formation in the membrane of *K. pneumoniae* and ROS overproduction. So, it is possible to correlate the ROS overproduction induced by Mo-CBP₃-PepI in *K. pneumoniae* cells with the pore that was formed.

3.3.2. Scanning Electron Microscopy (SEM)

SEM analysis was employed to provide more insights into the effect of Mo-CBP₃-PepI on *K. pneumoniae* morphology (Figure 4). As expected, control *K. pneumoniae* cells treated with DMSO presented a healthy morphology with no damage on the surface (Figure 4A).

However, *Mo*-CBP₃-PepI-treated *K. pneumoniae* cells presented several lethal damages on the surface (Figure 4B–H). After treatment with *Mo*-CBP₃-PepI, *K. pneumoniae* cells presented cells completely broken with damage to the cell wall, such as depressions, abnormal morphology, roughness, and an irregular cell surface (Figure 4B,C—white arrows), and in many cases, it is possible to see that the extravasation of cytoplasmic content may occur due to the pores formed in the membrane (Figure 4D–F,H—white arrows). Interestingly, *Mo*-CBP₃-PepI-treated *K. pneumoniae* cells presented structure-like depressions, broken cell walls, and contorted cells (Figure 4G).

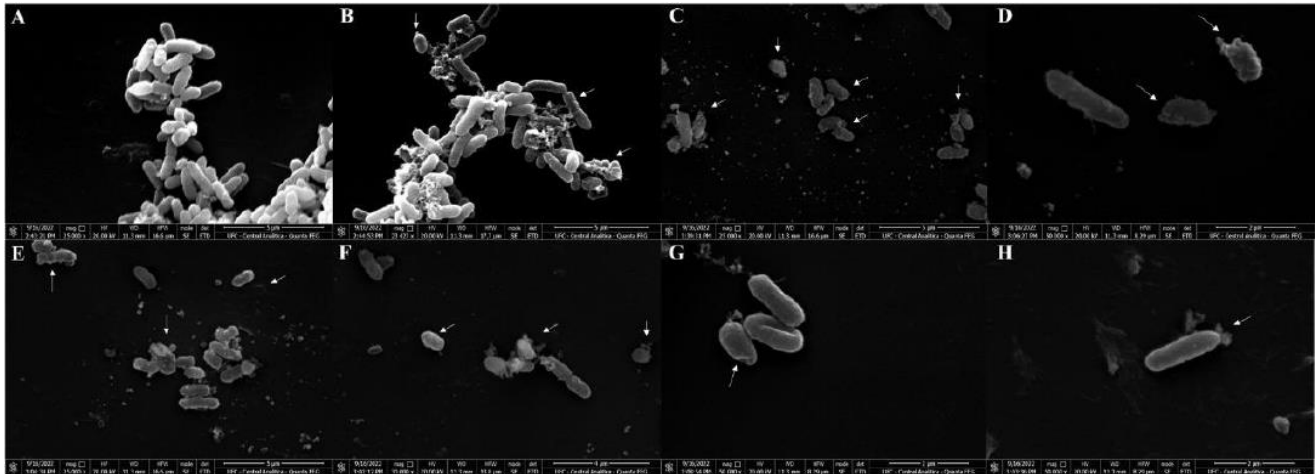


Figure 4. Scanning electron microscope of *K. pneumoniae* cells treated with *Mo*-CBP₃-PepI. (A) control *K. pneumoniae* cells treated with DMSO-NaCl solution. (B–H) *K. pneumoniae* cells treated with *Mo*-CBP₃-PepI 31.26 µg mL^{−1}.

SEM analysis corroborates the damage suggested by fluorescence microscopy. As revealed by fluorescence microscopy, *K. pneumoniae* cells present pores in the membrane after treatment with *Mo*-CBP₃-PepI. SEM analysis revealed several areas of damage to the structure of *K. pneumoniae*, including the loss of internal content mediated by pores. *Mo*-CBP₃-PepI induced the same damage in *Candida* cells [16]. For example, *Mo*-CBP₃-PepIII, a closely related peptide of *Mo*-CBP₃-PepI, also damaged the morphology of *Staphylococcus aureus* [15].

3.4. Proteomic Profile of *K. pneumoniae* Cells Treated with *Mo*-CBP₃-PepI

3.4.1. Overview

Proteomic analysis is a powerful technique employed to provide an overview of what happens in cells after treatment with peptides [35–39]. The proteomic response to peptides has been analyzed in *Escherichia coli* K12 [40], *Bacillus subtilis* [35], and *Clostridioides difficile* [38]. In many cases, proteomic analysis has been performed to understand the behavior of the multidrug-resistant bacteria's response to antibiotics [36]. Here, proteomic analysis was employed to overview protein changes in *K. pneumoniae* after treatment with *Mo*-CBP₃-PepI. In total, 547 were successfully identified (Figure 5). In total, 279 proteins were identified in *Mo*-CBP₃-PepI-treated *K. pneumoniae* cells and 268 in control *K. pneumoniae* cells (Figure 3A; Tables S1 and S2). Among exclusive proteins, 232 unique proteins were from *Mo*-CBP₃-PepI-treated *K. pneumoniae* cells and 221 were unique from control *K. pneumoniae* cells (Figure 5A; Tables S1 and S2).

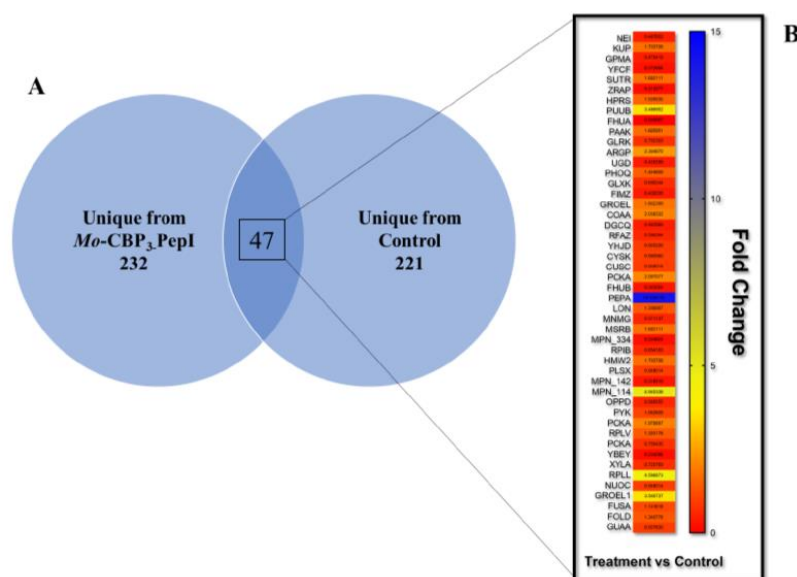


Figure 5. Distribution of *K. pneumoniae* proteins obtained after treatment with *Mo*-CBP₃-PepI. (A) Venn diagram shows the dispersion of total proteins of control and *Mo*-CBP₃-PepI-treated cells. (B) Represents the fold-change value of overlapping proteins, which were found in both groups. The vertical bar indicates the color scale according to each protein's fold-change value.

Besides the unique proteins, which are those exclusively found in one group, there were proteins detected in both groups, and they were shared proteins. To understand the patterns of differential accumulation of these proteins, a fold-change rule was applied, taking into account the intensity of protein *Mo*-CBP₃-PepI/Control *K. pneumoniae* cells.

Among the overlapping proteins, which were found in both groups, proteins with a fold-change value ≥ 1.5 ($p < 0.05$, Tukey's test) [41] were considered up-accumulated (increased the abundance), and proteins with a fold-change value ≤ 0.5 ($p < 0.05$, Tukey's test) were considered down-accumulated (decreased the abundance). For example, endonuclease 8 has a fold-change value of 0.287 and considered with a reduced abundance in cells treated with *Mo*-CBP₃-PepI compared to control cells.

Forty-seven proteins common to both groups, 19 up-accumulated, 19 down-accumulated, and 9 did not change when comparing *Mo*-CBP₃-PepI-treated with control cells (Figure 5B).

The Gene ontology classification of proteins shared by *Mo*-CBP₃-PepI- and control- *K. pneumoniae* cells revealed 11 and 16 groups of proteins, respectively, for biological activity and molecular function (Figure 6). Regarding the biological activity, the group that held the highest number of identified proteins was Energy and Metabolism with 36% of total proteins and the DNA metabolism group held the lowest number with 2% of the total identified proteins (Figure 6). In the case of molecular function, the transferase group possessed the highest amount, 26%, of identified proteins. Many groups, such as chaperone and ion binding, have a small number of proteins, 2% of the total identified included (Figure 6).

The protein groups involved in regulating transcription, transmembrane transporters, stress, and Defense Response, Energy and Metabolism, Pathogenesis, Protein Biosynthesis, Metabolism, Cell wall organization, and structural maintenance and transferase were composed of proteins that are both up- and down-accumulated (Table 2). In contrast, the groups Regulation Factor and RNA Processing and DNA metabolism are composed of proteins that decrease the abundance in *K. pneumoniae* cells after treatment with *Mo*-CBP₃-PepI (Table 2 and Figure 5B—Fold-Change). On the other hand, the downregulated proteins were related to regulation factors and transferase (Figure 5B—Fold-Change).

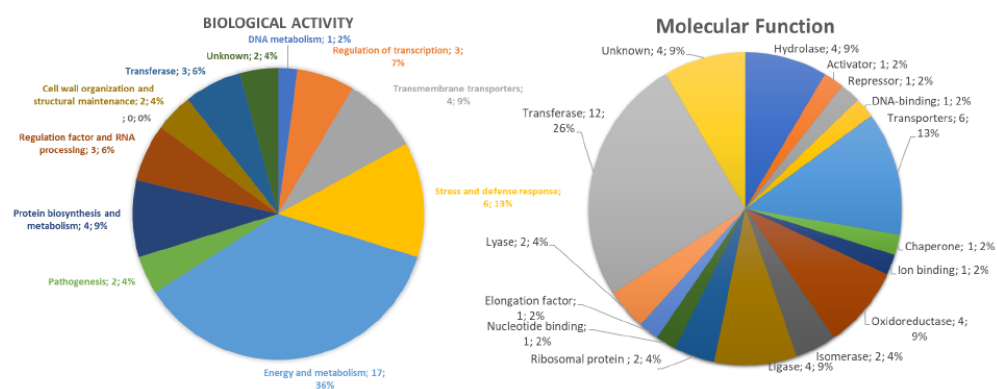


Figure 6. Classification proteins from *K. pneumoniae* cells identified by LC-ESI-MS/MS analysis. The overlapping proteins (found in both control and treated) were classified based on biological process and molecular function.

Table 2. Differentially accumulated proteins identified by ESI-LC-MS/MS.

Protein Name	ID (Uniprot)	Organism Reference	Cellular Compartment	Fold Change Mo-CBP ₃ -PepI vs. DMSO
DNA metabolism				
Endonuclease 8	P50465	<i>Escherichia coli</i> (strain K12)	Cytoplasm	0.287
Regulation of transcription				
HTH-type transcriptional regulator SutR	P77626	<i>Escherichia coli</i> (strain K12)	Cytoplasm	2.566
HTH-type transcriptional regulator ArgP	P0A8S1	<i>Escherichia coli</i> (strain K12)	Cytoplasm	2.364
Fimbriae Z protein	P0AEL8	<i>Escherichia coli</i> (strain K12)	Cytoplasm	0.690
Transmembrane transporters				
Low affinity potassium transport system protein kup	P63183	<i>Escherichia coli</i> (strain K12)	Plasma membrane	1.704
Ferrichrome outer membrane transporter/phage receptor	P06971	<i>Escherichia coli</i> (strain K12)	Plasma membrane	1.063
Cation efflux system protein CusC	P77211	<i>Escherichia coli</i> (strain K12)	cell outer membrane	0.920
Iron (3+)-hydroxamate import system permease protein FhuB	P06972	<i>Escherichia coli</i> (strain K12)	Plasma membrane	0.948
Stress and Defense Response				
Zinc resistance-associated protein	P0AAA9	<i>Escherichia coli</i> (strain K12)	Periplasm space	1.682
Chaperonin GroEL	P0A6F5	<i>Escherichia coli</i> (strain K12)	Cytoplasm	1.444
Undecaprenyl-diphosphatase	Q2KX31	<i>Bordetella avium</i> (strain 197N)	Plasma membrane	1.340
Peptide methionine sulfoxide reductase MsrB	P75129	<i>Mycoplasma pneumoniae</i> (strain ATCC 29342/M129)	Cytoplasm	14.104
Periplasmic trehalase	Q4UZ12	<i>Xanthomonas campestris pv. campestris</i> (strain 8004)	Periplasmic space	0.937
Lon protease	P78025	<i>Mycoplasma pneumoniae</i> (strain ATCC 29342/M129)	Cytoplasm	0.342
Energy and Metabolism				
2,3-bisphosphoglycerate-dependent phosphoglycerate mutase	P62707	<i>Escherichia coli</i> (strain K12)	Cytoplasm	0.519
Gamma-glutamylputrescine oxidoreductase	P37906	<i>Escherichia coli</i> (strain K12)	Cytoplasm	0.985
2-succinyl-5-enolpyruvyl-6-hydroxy-3-cyclohexene-1-carboxylate synthase	P17109	<i>Escherichia coli</i> (strain K12)	Plasma membrane	3.486
UDP-glucose 6-dehydrogenase	P76373	<i>Escherichia coli</i> (strain K12)	Cytoplasm	0.902
Glycerate 3-kinase	P77364	<i>Escherichia coli</i> (strain K12)	Cytoplasm	0.745
Phenylacetate-coenzyme A ligase	P76085	<i>Escherichia coli</i> (strain K12)	Cytoplasm	1.666
Pantothenate kinase	P0A6I3	<i>Escherichia coli</i> (strain K12)	Cytoplasm	0.548

Table 2. Cont.

Protein Name	ID (Uniprot)	Organism Reference	Cellular Compartment	Fold Change Mo-CBP ₃ -PepI vs. DMSO
Pyruvate kinase	P78031	<i>Mycoplasma pneumoniae</i> (strain ATCC 29342/M129)	Membrane	3.139
Phosphoenolpyruvate carboxykinase (ATP)	A8AQV7	<i>Escherichia coli</i> (strain K12)	Cytoplasm	0.990
Xylose isomerase	B5ZQV6	<i>Rhizobium leguminosarum</i> <i>bv. trifolii</i> (strain WSM2304)	Cytoplasm	1.062
Bifunctional protein Fold	Q88WM8	<i>Lactiplantibacillus plantarum</i> (strain ATCC BAA-793/NCIMB 8826/WCFS1)	Periplasmic space	0.726
GMP synthase (glutamine-hydrolyzing)	Q6APU2	<i>Desulfotalea psychrophila</i> (strain LSV54/DSM 12343)	Cytoplasm	4.596
Sensor histidine kinase GlrK	P52101	<i>Escherichia coli</i> (strain K12)	Cell inner membrane	0.752
Sensor protein PhoQ	P23837	<i>Escherichia coli</i> (strain K12)	Plasma membrane	0.823
Putative ABC transporter ATP-binding protein MPN_334	P75444	<i>Mycoplasma pneumoniae</i> (strain ATCC 29342/M129)	Plasma membrane	1.336
Oligopeptide transport ATP-binding protein OppD	P75552	<i>Mycoplasma pneumoniae</i> (strain ATCC 29342/M129)	Plasma membrane	0.948
Pantothenate synthetase	B81Z3	<i>Ruminiclostridium cellulolyticum</i> (strain ATCC 35319/DSM 5812/JCM 6584/H10)	Cytoplasm	1.142
Pathogenesis				
Lipopolysaccharide core biosynthesis protein RfaZ	P27241	<i>Escherichia coli</i> (strain K12)	Cytoplasm	2.038
Inner membrane protein YhjD	P37642	<i>Escherichia coli</i> (strain K12)	Plasma membrane	0.362
Protein Biosynthesis and Metabolism				
50S ribosomal protein L22	A5IYY1	<i>Mycoplasma agalactiae</i>	Large ribosomal subunit	0.187
50S ribosomal protein L7/L12	P0A466	<i>Aquifex aeolicus</i> (strain VF5)	Large ribosomal subunit	1.979
Diaminopimelate decarboxylase	Q8K9C4	<i>Buchnera aphidicola</i> subsp. <i>Schizaphis graminum</i> (strain Sg)	Cytoplasm	3.546
Cysteine synthase A	P0ABK5	<i>Escherichia coli</i> (strain K12)	Cytoplasm	0.596
Regulation Factor and RNA Processing				
tRNA uridine 5-carboxymethylaminomethyl modification enzyme MnmG	P75221	<i>Mycoplasma pneumoniae</i> (strain ATCC 29342/M129)	Cytoplasm	0.487
Elongation factor G	Q7NAV3	<i>Mycoplasma gallisepticum</i> (strain R(low/passage 15/clone 2))	Cytoplasm	0.234
Methylenetetrahydrofolate-tRNA-(uracil-5-)-methyltransferase TrmFO	A4WRQ2	<i>Cereibacter sphaeroides</i> (strain ATCC 17025/ATH 2.4.3)	Cytoplasm	0.948
Cell wall organization and structural maintenance				
Cytadherence high molecular weight protein 2	P75471	<i>Mycoplasma pneumoniae</i> (strain ATCC 29342/M129)	Cytoplasm	1.682
Mgp-operon protein 3	Q50341	<i>Mycoplasma pneumoniae</i> (strain ATCC 29342/M129)	Plasma membrane	0.654
Transferase				
Glutathione S-transferase YfcF	P77544	<i>Escherichia coli</i> (strain K12)	Cytoplasm	0.273
Phosphate acyltransferase	P75232	<i>Mycoplasma pneumoniae</i> (strain ATCC 29342/M129)	Cytoplasm	3.096
Sensor histidine kinase HprS	P76339	<i>Escherichia coli</i> (strain K12)	Plasma membrane	0.213

Table 2. Cont.

Protein Name	ID (Uniprot)	Organism Reference	Cellular Compartment	Fold Change <i>Mo</i> -CBP ₃ -PepI vs. DMSO
Unknown				
Probable cytosol aminopeptidase	P75206	<i>Mycoplasma pneumoniae</i> (strain ATCC 29342/M129)	Cytoplasm	2.097
Putative acetyltransferase MPN_114	P75448	<i>Mycoplasma pneumoniae</i> (strain ATCC 29342/M129)	Unknown	1.703

3.4.2. DNA Metabolism-Related Proteins

In this group, one protein was found in both *Mo*-CBP₃-PepI and DMSO groups, Endonuclease 8 (Table 2), which was down-accumulated in *K. pneumoniae* cells treated with *Mo*-CBP₃-PepI compared to DMSO cells (control). Endonuclease 8 is an enzyme involved in the DNA repair process after damage by oxidation by ROS [42–44]. The reduction in the abundance of Endonuclease 8 in cells treated with *Mo*-CBP₃-PepI is attractive because it noticed a higher accumulation of ROS (Figure 3) in those cells. So, the high accumulation of ROS and reduction in accumulation of the Endonuclease 8 suggest that DNA from *K. pneumoniae* cells is being damaged by ROS induced by *Mo*-CBP₃-PepI [26].

The proteins UvrA, UvrB, and UvrC, were exclusive from *K. pneumoniae* cells treated with *Mo*-CBP₃-PepI (Table S1). Based on that, it is feasible to suggest that *Mo*-CBP₃-PepI induced damage in the DNA of *K. pneumoniae* because these enzymes repair both strands of DNA [45]. Interestingly, only in the control cells (Table S2), but not in treated cells, the protein DNA repair protein RecN was detected as the cell's first line to protect the DNA from damage [46]. Somehow, *Mo*-CBP₃-PepI induces a down-accumulation in *K. pneumoniae* cells that, combined with ROS accumulation, leads to DNA damage and cell death.

3.4.3. Stress and Defense Response Related Proteins

In this group, one protein deserved attention, Peptide methionine sulfoxide reductase MsrB was highly accumulated in *K. pneumoniae* cells treated with *Mo*-CBP₃-PepI compared to control cells with a fold-change value of 14.104 (Table 2). The MsrB protein is a highly conserved protein essential in the cell defense mechanism against high ROS levels, and it works in the repair of inactivated protein by ROS [47]. The increase in MsrB in cells treated with *Mo*-CBP₃-PepI compared to control agrees with the high accumulation of ROS in cells (Figure 3). Proteins and other vital molecules in the cell are attacked and inactivated by ROS [26]. The increased abundance of MsrB protein indicates severe damage in proteins of *K. pneumoniae* cells after treatment with *Mo*-CBP₃-PepI and that cells are trying to recover from this stress. The MsrB proteins are involved in recovering proteins oxidized by ROS species [26].

Proteomic analysis of cells revealed a reduction in the accumulation of an important protein, Lon protease, in cells treated with *Mo*-CBP₃-PepI compared to control cells (Table 2). Lon protease is a multifunctional, highly conserved ATP-dependent serine protease involved in protein turnover in bacterial cells [48,49]. Lon protease degrades either natural or ROS-induced misfolded proteins leading to free amino acids to produce new functional proteins [48,50]. The reduction in the abundance of Lon protease in *Mo*-CBP₃-PepI-treated cells may suggest an accumulation of misfolded proteins that mitigate the chance of responding to the stress imposed by *Mo*-CBP₃-PepI. Additionally, the Lon protease is essential to encapsulation, motility, heat-shock response, persister formation and drug resistance, and virulence factor production [51–56]. By inducing the reduction in accumulation of Lon protease in *K. pneumoniae* cells, *Mo*-CBP₃-PepI dramatically reduced the chances of the cell to respond to stress and inhibit several essential processes to cell normal function leading to death.

The proteins unique from control cells were identified, such as multidrug resistance protein MdtN, UPF0194 membrane protein YbhG, and multidrug resistance protein EmrK (Table S2). MdtN is a protein involved in the resistance against puromycin and acriflavine [55], EmrK is a part of the efflux pump involved in multidrug resistance [57], and YbhG is involved in resistance to chloramphenicol [58]. This is an exciting result because the absence of these in the *Mo-CBP3-PepI*-treated cells indicates that they became susceptible to these antibiotics again, which is an important outcome.

3.4.4. Protein Biosynthesis and Metabolism Related Proteins

The analysis of proteins related to protein biosynthesis and metabolism revealed a quite complex scenario in *K. pneumoniae* cells after treatment with *Mo-CBP3-PepI* (Table 2; Tables S1 and S2). For example, among the overlapping proteins, the 50S ribosomal protein L22 and 50S ribosomal protein L7/L12, respectively, showed a reduction and increased abundance in *K. pneumoniae* cells treated with *Mo-CBP3-PepI* compared to control cells (Table 2). The 50S ribosomal protein L22 is a vital core protein of bacterial ribosomes involved in the aggregation and stabilization of ribosomal proteins to form the ribosome in bacteria [59,60]. The L22 subunit is so important to bacterial ribosomes that it is the target of antibiotics such as macrolides [59,60]. The reduction in abundance in this protein induced by *Mo-CBP3-PepI* indicates a destabilization of bacterial ribosomes leading to the inhibition of protein synthesis in bacteria.

An increase in the abundance of 50S ribosomal protein L7/L12 in cells treated with *Mo-CBP3-PepI* (Table 2) was seen, compared to the control. The increase in this protein is perhaps a mechanism of the cell to supply the deficiency of the ribosomal protein L22. However, the L7/L12 is a GTPase protein involved in the process such as translation initiation, elongation, and termination by the mature 70S ribosome [61]. However, increasing this protein will not help cells perform protein synthesis without the L22 subunit.

An interesting result came out by evaluating the unique proteins, *Mo-CBP3-PepI* and control cells (Tables 1 and 2). Among the proteins exclusively detected in *K. pneumoniae* cells treated with *Mo-CBP3-PepI* are Cysteine-tRNA ligase, Leucine-tRNA ligase, Serine-tRNA ligase, Valine-tRNA ligase, Glutamine-tRNA, Phenylalanine-tRNA ligase alpha subunit, Valine-tRNA ligase, Proline-tRNA ligase, Alanine-tRNA ligase, and Threonine-tRNA ligase (Table S1). All these proteins are involved in amino acid delivery to ribosomes during protein synthesis. The increase in these proteins' abundance indicates a cell attempt to either increase or maintain the protein synthesis at normal levels to allow cells to fight back against insults imposed by *Mo-CBP3-PepI*.

Proteins are important to all living organisms, and bacteria must understand what is happening in their environment to respond accordingly. Proteins make all this happen. To respond to stress agents, such as *Mo-CBP3-PepI*, *K. pneumoniae* must reprogram all its protein profiles to produce defense proteins [62]. For example, *K. pneumoniae* cells should produce scavenger proteins to defend themselves from ROS overproduction, but that is impossible. That happens because *Mo-CBP3-PepI* reduced the abundance of an important protein for ribosomal activity. As a consequence, *K. pneumoniae* cells could not produce scavenger proteins, thus leading to ROS accumulation and damage to DNA (as reported above) and damage to other proteins leading the cell to death as revealed by the damage present in fluorescence and scanning electron microscopy.

3.4.5. Regulation Factor and RNA Processing Related Proteins

In this group of proteins, the protein elongation factor (Q7NAV3) G that decreases in abundance in *K. pneumoniae* treated with *Mo-CBP3-PepI* deserves attention (Table 2). By looking into unique proteins from control cells (Table S2), one isoform of elongation factor G (Q492B1) and other factors, such as Elongation factor Tu 1 and Elongation factor 4, are present but disappear completely in treated versus control cells. Elongation factor G is important for the translocation process during prokaryotic protein synthesis, and it uses the energy held in GTP to interact with tRNA and mRNA [63]. The decrease in the abundance

of Elongation factor G led to the shutdown of protein synthesis in *K. pneumoniae* cells. As discussed above in the protein metabolism section, the protein synthesis in *K. pneumoniae* cells is dramatically affected by Mo-CBP3-PepI, giving them no chance to respond to the stress imposed by the peptide.

3.4.6. Cell Wall Organization and Structure Maintenance Related Proteins

In this group of proteins, important proteins were exclusively found in *K. pneumoniae* cells treated with Mo-CBP3-PepI (Table S1), which are soluble lytic murein transglycosylase, D-alanyl-D-alanine carboxypeptidase DacB, Cell shape-determining protein MreB, Probable L, D-transpeptidase ErfK/SrfK, Cell shape-determining protein MreC, Murein tetrapeptide carboxypeptidase, Murein DD-endopeptidase MepH, Sensor protein LytS, D-alanine-D-alanine ligase, and Inner membrane protein YdcZ. All are involved in cell wall turnover, cell structure maintenance, and shape stabilization [64–66]. The increased abundance of these proteins indicates that *K. pneumoniae* cells are suffering from stress in the cell wall imposed by Mo-CBP3-PepI and are trying to overcome the stress. However, as revealed by SEM analysis (Figure 4), *K. pneumoniae* cells treated with Mo-CBP3-PepI presented damage to the cell wall and cell morphology. It has been related that Mo-CBP3-PepI can bind to the cell wall of the yeast *C. albicans* [16].

The bacterial cell wall is a crucial component of the cell involved in mechanical defense against several environmental stresses [67]. During stress, the cell must recover the cell wall every time that damage occurs. The exclusive detection of this protein in cells treated with Mo-CBP3-PepI indicates that it is imposing stress on the cell wall and is trying to recover, but as revealed by microscopic analysis (Figures 3 and 4).

3.4.7. Transferase-Related Proteins

In this group, one protein is relevant, the sensor histidine kinase HprS, which presented a reduced abundance in cells treated with Mo-CBP3-PepI compared to the control cells (Table 2). Histidine kinase sensors are environmental elements employed by bacteria to sense the environment and respond accordingly [68,69]. These sensors are mainly responsible for perceiving and responding to oxidative stress [70]. Here, the reduction in the abundance of HprS agreed with the high accumulation of ROS (Figure 3) in *K. pneumoniae* cells treated with Mo-CBP3-PepI. This result shows that Mo-CBP3-PepI imposes two stresses on *K. pneumoniae* cells. First is the induction of accumulation of ROS at higher levels; second is the reduction in the protein accumulation involved in the perception and response of stress caused by ROS. In this case, Mo-CBP3-PepI simultaneously induces stress and inhibits the cell's ability to develop a response to it.

3.4.8. Cell Redox Homeostasis-Related Proteins

This group is particularly important given the scenario of high levels of ROS accumulation in *K. pneumoniae* cells induced by Mo-CBP3-PepI. In this group, where no overlapping proteins found, only exclusive proteins either from Mo-CBP3-PepI-treated or control *K. pneumoniae* cells (Tables S1 and S2). For example, Alkyl hydroperoxide reductase C and Alkyl hydroperoxide reductase subunit F were only detected in control *K. pneumoniae* (Table S2). Thiol-peroxidases are responsible for the scavenging of H₂O₂, protecting the bacterial cell from toxic levels of endogenously H₂O₂ [71,72].

Interestingly, these enzymes were not detected in cells treated with Mo-CBP3-PepI, indicating a complete depletion of these enzymes. The absence of these enzymes in treated cells might lead to the accumulation of H₂O₂ (Figure 3), as revealed by fluorescence microscopy. To cope with the high levels of ROS induced by peptides, *K. pneumoniae* cells increase the abundance of a catalase-peroxidase enzyme, only detected in treated cells, which is involved in the defense mechanism against high levels of ROS [71]. Our data revealed that even though *K. pneumoniae* cells treated with Mo-CBP3-PepI increased the abundance of a catalase enzyme to remove the excess ROS, those scavenger enzymes are not enough to prevent the damage produced by high levels of H₂O₂ once microscopic

Author Contributions: All authors made substantial contributions. The conception and design of the study and acquisition of data, analysis, and interpretation were performed by L.A.C.B., P.F.N.S., N.A.S.N., T.K.B.A., A.F.B.S., R.F.C., C.S.N., F.P.M., L.B.L. and C.D.T.F.; Microscopic analyses were carried out by L.A.C.B., P.F.N.S., N.A.S.N. and T.K.B.A.; Writing or revising the article was completed by L.A.C.B. and P.F.N.S.; P.F.N.S. completed the final approval and submission. All authors have read and agreed to the published version of the manuscript.

Funding: Special thanks to CAPES for providing the postdoctoral grant to Pedro F. N. Souza (grant number 88887.318820/2019-00).

Institutional Review Board Statement: Not applicable.

Informed Consent Statement: Not applicable.

Data Availability Statement: The data supporting this study's findings are available on request from the corresponding author.

Acknowledgments: We are also grateful to the staff of the central analytical facilities of UFC, Brazil.

Conflicts of Interest: The authors report no conflict of interest. The authors alone are responsible for the content and the writing of the paper.

References

1. O'Neill, J. *Tackling Drug-Resistant Infections Globally: Final Report and Recommendations*; Government of the United Kingdom: London, UK, 2016.
2. About Antibiotic Resistance | CDC. Available online: <https://www.cdc.gov/drugresistance/about.html> (accessed on 11 November 2022).
3. Murray, C.J.; Ikuta, K.S.; Sharara, F.; Swetschinski, L.; Robles Aguilar, G.; Gray, A.; Han, C.; Bisignano, C.; Rao, P.; Wool, E.; et al. Global Burden of Bacterial Antimicrobial Resistance in 2019: A Systematic Analysis. *Lancet* **2022**, *399*, 629–655. [[CrossRef](#)]
4. Klebsiella Pneumoniae in Healthcare Settings | HAI | CDC. Available online: <https://www.cdc.gov/hai/organisms/klebsiella/klebsiella.html> (accessed on 11 November 2022).
5. Mulani, M.S.; Kamble, E.E.; Kumkar, S.N.; Tawre, M.S.; Pardesi, K.R. Emerging Strategies to Combat ESKAPE Pathogens in the Era of Antimicrobial Resistance: A Review. *Front. Microbiol.* **2019**, *10*, 539. [[CrossRef](#)]
6. De Oliveira, D.M.P.; Forde, B.M.; Kidd, T.J.; Harris, P.N.A.; Schembri, M.A.; Beatson, S.A.; Paterson, D.L.; Walker, M.J. Antimicrobial Resistance in ESKAPE Pathogens. *Clin. Microbiol. Rev.* **2020**, *33*, e00181-19. [[CrossRef](#)]
7. Livermore, D.M.; Macgowan, A.P.; Wale, M.C.J. *Surveillance of Antimicrobial Resistance*; World Health Organization: Geneva, Switzerland, 1998; Volume 317, ISBN 9789294983879.
8. Tzouveleki, L.S.; Markogiannakis, A.; Piperaki, E.; Souli, M.; Daikos, G.L. Treating Infections Caused by Carbapenemase-Producing Enterobacteriaceae. *Clin. Microbiol. Infect.* **2014**, *20*, 862–872. [[CrossRef](#)]
9. Zowawi, H.M.; Forde, B.M.; Alfaresi, M.; Alzarouni, A.; Farahat, Y.; Chong, T.M.; Yin, W.F.; Chan, K.G.; Li, J.; Schembri, M.A.; et al. Stepwise Evolution of Pandrug-Resistance in Klebsiella Pneumoniae. *Sci. Rep.* **2015**, *5*, 15082. [[CrossRef](#)]
10. McNeil, J.C.; Vallejo, J.G.; Hultén, K.G.; Kaplan, S.L. Osteoarticular Infections Following Open or Penetrating Trauma in Children in the Post-Community-Acquired Methicillin-resistant Staphylococcus aureus Era: The Impact of Enterobacter cloacae. *Pediatr. Infect. Dis. J.* **2018**, *37*, 1204–1210. [[CrossRef](#)]
11. Corey, G.R.; Arhin, F.F.; Wikler, M.A.; Sahm, D.F.; Kreiswirth, B.N.; Mediavilla, J.R.; Good, S.; Fiset, C.; Jiang, H.; Moeck, G.; et al. Pooled Analysis of Single-Dose Oritavancin in the Treatment of Acute Bacterial Skin and Skin-Structure Infections Caused by Gram-Positive Pathogens, Including a Large Patient Subset with Methicillin-Resistant Staphylococcus Aureus. *Int. J. Antimicrob. Agents* **2016**, *48*, 528–534. [[CrossRef](#)]
12. Rubinstein, E.; Kollef, M.H.; Nathwani, D. Pneumonia Caused by Methicillin-Resistant Staphylococcus Aureus. *Clin. Infect. Dis.* **2008**, *46*, S378–S385. [[CrossRef](#)]
13. Lima, A.M.; Azevedo, M.I.G.; Sousa, L.M.; Oliveira, N.S.; Andrade, C.R.; Freitas, C.D.T.; Souza, P.F.N. Plant Antimicrobial Peptides: An Overview about Classification, Toxicity and Clinical Applications. *Int. J. Biol. Macromol.* **2022**, *214*, 10–21. [[CrossRef](#)]
14. Souza, P.F.N.; Marques, L.S.M.; Oliveira, J.T.A.; Lima, P.G.; Dias, L.P.; Neto, N.A.S.; Lopes, F.E.S.; Sousa, J.S.; Silva, A.F.B.; Caneiro, R.F.; et al. Synthetic Antimicrobial Peptides: From Choice of the Best Sequences to Action Mechanisms. *Biochimie* **2020**, *175*, 132–145. [[CrossRef](#)]
15. Oliveira, J.T.A.; Souza, P.F.N.; Vasconcelos, I.M.; Dias, L.P.; Martins, T.F.; Van Tilburg, M.F.; Guedes, M.I.F.; Sousa, D.O.B. Mo-CBP3-PepI, Mo-CBP3-PepII, and Mo-CBP3-PepIII Are Synthetic Antimicrobial Peptides Active against Human Pathogens by Stimulating ROS Generation and Increasing Plasma Membrane Permeability. *Biochimie* **2019**, *157*, 10–21. [[CrossRef](#)] [[PubMed](#)]
16. Lima, P.G.; Souza, P.F.N.; Freitas, C.D.T.; Oliveira, J.T.A.; Dias, L.P.; Neto, J.X.S.; Vasconcelos, I.M.; Lopes, J.L.S.; Sousa, D.O.B. Anticandidal Activity of Synthetic Peptides: Mechanism of Action Revealed by Scanning Electron and Fluorescence Microscopies and Synergism Effect with Nystatin. *J. Pept. Sci.* **2020**, *26*, e3249. [[CrossRef](#)] [[PubMed](#)]

17. Souza, P.F.N.; Lima, P.G.; Freitas, C.D.T.; Sousa, D.O.B.; Neto, N.A.S.; Dias, L.P.; Vasconcelos, I.M.; Freitas, L.B.N.; Silva, R.G.G.; Sousa, J.S.; et al. Antidermatophytic Activity of Synthetic Peptides: Action Mechanisms and Clinical Application as Adjuvants to Enhance the Activity and Decrease the Toxicity of Griseofulvin. *Mycoses* **2020**, *63*, 979–992. [[CrossRef](#)] [[PubMed](#)]
18. Neto, N.A.S.; Oliveira, J.T.A.; Aguiar, T.K.B.; Bezerra, L.P.; Branco, L.A.C.; Mesquita, F.P.; Freitas, C.D.T.; Souza, P.F.N. Synergistic Antibiofilm Activity between Synthetic Peptides and Ciprofloxacin against *Staphylococcus Aureus*. *Pathogens* **2022**, *11*, 995. [[CrossRef](#)] [[PubMed](#)]
19. Lima, P.G.; Freitas, C.D.T.; Oliveira, J.T.A.; Neto, N.A.S.; Amaral, J.L.; Silva, A.F.B.; Sousa, J.S.; Franco, O.L.; Souza, P.F.N. Synthetic Antimicrobial Peptides Control *Penicillium Digitatum* Infection in Orange Fruits. *Food Res. Int.* **2021**, *147*, 110582. [[CrossRef](#)] [[PubMed](#)]
20. Staniszewska, M.; Bondaryk, M.; Swoboda-Kopec, E.; Siennicka, K.; Sygitowicz, G.; Kurzatkowski, W. *Candida Albicans* Morphologies Revealed by Scanning Electron Microscopy Analysis. *Braz. J. Microbiol.* **2013**, *44*, 813–821. [[CrossRef](#)] [[PubMed](#)]
21. Fleeman, R.M.; Macias, L.A.; Brodbelt, J.S.; Davies, B.W. Defining Principles That Influence Antimicrobial Peptide Activity against Capsulated *Klebsiella Pneumoniae*. *Proc. Natl. Acad. Sci. USA* **2020**, *117*, 27620–27626. [[CrossRef](#)]
22. Tincho, M.B.; Morris, T.; Meyer, M.; Pretorius, A. Antibacterial Activity of Rationally Designed Antimicrobial Peptides. *Int. J. Microbiol.* **2020**, *2020*, 2131535. [[CrossRef](#)]
23. Jindal, H.M.; Le, C.F.; Yusof, M.Y.M.; Velayuthan, R.D.; Lee, V.S.; Zain, S.M.; Isa, D.M.; Sekaran, S.D. Antimicrobial Activity of Novel Synthetic Peptides Derived from Indolicidin and Ranalexin against *Streptococcus Pneumoniae*. *PLoS ONE* **2015**, *10*, e0128532. [[CrossRef](#)]
24. Parra, A.L.C.; Freitas, C.D.T.; Souza, P.F.N.; von Aderkas, P.; Borchers, C.H.; Beattie, G.A.; Silva, F.D.A.; Thornburg, R.W. Ornamental Tobacco Floral Nectar Is a Rich Source of Antimicrobial Peptides. *Plant Sci.* **2022**, *324*, 111427. [[CrossRef](#)]
25. Aguiar, T.K.B.; Neto, N.A.S.; Freitas, C.D.T.; Silva, A.F.B.; Bezerra, L.P.; Malveira, E.A.; Branco, L.A.C.; Mesquita, F.P.; Goldman, G.H.; Alencar, L.M.R.; et al. Antifungal Potential of Synthetic Peptides against *Cryptococcus Neoformans*: Mechanism of Action Studies Reveal Synthetic Peptides Induce Membrane–Pore Formation, DNA Degradation, and Apoptosis. *Pharmaceutics* **2022**, *14*, 1678. [[CrossRef](#)] [[PubMed](#)]
26. Wang, K.; Dang, W.; Xie, J.; Zhu, R.; Sun, M.; Jia, F.; Zhao, Y.; An, X.; Qiu, S.; Li, X.; et al. Antimicrobial Peptide Protonection Disturbs the Membrane Integrity and Induces ROS Production in Yeast Cells. *Biochim. Biophys. Acta-Biomembr.* **2015**, *1848*, 2365–2373. [[CrossRef](#)] [[PubMed](#)]
27. Lee, M.T.; Hung, W.C.; Chen, F.Y.; Huang, H.W. Mechanism and Kinetics of Pore Formation in Membranes by Water-Soluble Amphipathic Peptides. *Proc. Natl. Acad. Sci. USA* **2008**, *105*, 5087–5092. [[CrossRef](#)]
28. Lima, P.G.; Oliveira, J.T.A.; Amaral, J.L.; Freitas, C.D.T.; Souza, P.F.N. Synthetic Antimicrobial Peptides: Characteristics, Design, and Potential as Alternative Molecules to Overcome Microbial Resistance. *Life Sci.* **2021**, *278*, 119647. [[CrossRef](#)] [[PubMed](#)]
29. Hristova, K.; Wimley, W.C. A Look at Arginine in Membranes. *J. Membr. Biol.* **2011**, *239*, 49. [[CrossRef](#)]
30. Campelo, F.; McMahon, H.T.; Kozlov, M.M. The Hydrophobic Insertion Mechanism of Membrane Curvature Generation by Proteins. *Biophys. J.* **2008**, *95*, 2325–2339. [[CrossRef](#)]
31. Huang, Y.; Huang, J.; Chen, Y. Alpha-Helical Cationic Antimicrobial Peptides: Relationships of Structure and Function. *Protein Cell* **2010**, *1*, 143–152. [[CrossRef](#)]
32. Shai, Y. Mechanism of the Binding, Insertion and Destabilization of Phospholipid Bilayer Membranes by Alpha-Helical Antimicrobial and Cell Non-Selective Membrane-Lytic Peptides. *Biochim. Biophys. Acta* **1999**, *1462*, 55–70. [[CrossRef](#)]
33. Jean-François, F.; Elezgaray, J.; Berson, P.; Vacher, P.; Dufourc, E.J. Pore Formation Induced by an Antimicrobial Peptide: Electrostatic Effects. *Biophys. J.* **2008**, *95*, 5748–5756. [[CrossRef](#)]
34. Rowe-Magnus, D.A.; Kao, A.Y.; Prieto, A.C.; Pu, M.; Kao, C. Cathelicidin Peptides Restrict Bacterial Growth via Membrane Perturbation and Induction of Reactive Oxygen Species. *mBio* **2019**, *10*, e02021-19. [[CrossRef](#)]
35. Wenzel, M.; Chiriac, A.I.; Otto, A.; Zweytick, D.; May, C.; Schumacher, C.; Gust, R.; Albada, H.B.; Penkova, M.; Krämer, U.; et al. Small Cationic Antimicrobial Peptides Delocalize Peripheral Membrane Proteins. *Proc. Natl. Acad. Sci. USA* **2014**, *111*, 1409–1418. [[CrossRef](#)] [[PubMed](#)]
36. Tsakou, F.; Jersie-Christensen, R.; Jenssen, H.; Mojsoska, B. The Role of Proteomics in Bacterial Response to Antibiotics. *Pharmaceutics* **2020**, *13*, 214. [[CrossRef](#)] [[PubMed](#)]
37. Moyer, T.B.; Purvis, A.L.; Wommack, A.J.; Hicks, L.M. Proteomic Response of *Escherichia Coli* to a Membrane Lytic and Iron Chelating Truncated *Amaranthus Tricolor* Defensin. *BMC Microbiol.* **2021**, *21*, 110. [[CrossRef](#)] [[PubMed](#)]
38. Maaß, S.; Bartel, J.; Mücke, P.A.; Schlüter, R.; Sura, T.; Zschke-Kriesche, J.; Smits, S.H.J.; Becher, D. Proteomic Adaptation of *Clostridioides Difficile* to Treatment with the Antimicrobial Peptide Nisin. *Cells* **2021**, *10*, 372. [[CrossRef](#)]
39. Senges, C.H.R.; Stepanek, J.J.; Wenzel, M.; Raatschen, N.; Ay, Ü.; Märten, Y.; Prochnow, P.; Hernández, M.V.; Yayci, A.; Schubert, B.; et al. Comparison of Proteomic Responses as Global Approach to Antibiotic Mechanism of Action Elucidation. *Antimicrob. Agents Chemother.* **2021**, *65*, e01373-20. [[CrossRef](#)] [[PubMed](#)]
40. Wang, H.; Xie, Y.; Zhang, H.; Jin, J.; Zhang, H. Quantitative Proteomic Analysis Reveals the Influence of Plantaricin BM-1 on Metabolic Pathways and Peptidoglycan Synthesis in *Escherichia Coli* K12. *PLoS ONE* **2020**, *15*, e0231975. [[CrossRef](#)] [[PubMed](#)]

41. Noronha Souza, P.F.; Abreu Oliveira, J.T.; Vasconcelos, I.M.; Magalhães, V.G.; Albuquerque Silva, F.D.; Guedes Silva, R.G.; Oliveira, K.S.; Franco, O.L.; Gomes Silveira, J.A.; Leite Carvalho, F.E. H₂O₂ Accumulation, Host Cell Death and Differential Levels of Proteins Related to Photosynthesis, Redox Homeostasis, and Required for Viral Replication Explain the Resistance of EMS-Mutagenized Cowpea to Cowpea Severe Mosaic Virus. *J. Plant Physiol.* **2020**, *245*, 153110. [[CrossRef](#)]
42. Burgess, S.; Jaruga, P.; Dodson, M.L.; Dizdaroglu, M.; Stephen Lloyd, R. Determination of Active Site Residues in Escherichia Coli Endonuclease VIII. *J. Biol. Chem.* **2002**, *277*, 2938–2944. [[CrossRef](#)]
43. Jiang, D.; Hatahet, Z.; Blaisdell, J.O.; Melamede, R.J.; Wallace, S.S. Escherichia Coli Endonuclease VIII: Cloning, Sequencing, and Overexpression of the Nei Structural Gene and Characterization of Nei and Nei Nth Mutants. *J. Bacteriol.* **1997**, *179*, 3773–3782. [[CrossRef](#)]
44. Oshima, T.; Aiba, H.; Baba, T.; Fujita, K.; Hayashi, K.; Honjo, A.; Ikemoto, K.; Inada, T.; Itoh, T.; Kajihara, M.; et al. A 718-Kb DNA Sequence of the Escherichia Coli K-12 Genome Corresponding to the 12.7–28.0 Min Region on the Linkage Map. *DNA Res.* **1996**, *3*, 137–155. [[CrossRef](#)]
45. Verhoeven, E.E.A.; Wyman, C.; Moolenaar, G.F.; Goosen, N. The Presence of Two UvrB Subunits in the UvrAB Complex Ensures Damage Detection in Both DNA Strands. *EMBO J.* **2002**, *21*, 4196–4205. [[CrossRef](#)] [[PubMed](#)]
46. Kidane, D.; Sanchez, H.; Alonso, J.C.; Graumann, P.L. Visualization of DNA Double-Strand Break Repair in Live Bacteria Reveals Dynamic Recruitment of Bacillus Subtilis RecF, RecO and RecN Proteins to Distinct Sites on the Nucleoids. *Mol. Microbiol.* **2004**, *52*, 1627–1639. [[CrossRef](#)] [[PubMed](#)]
47. Delaye, L.; Becerra, A.; Orgel, L.; Lazcano, A. Molecular Evolution of Peptide Methionine Sulfoxide Reductases (MsrA and MsrB): On the Early Development of a Mechanism That Protects against Oxidative Damage. *J. Mol. Evol.* **2007**, *64*, 15–32. [[CrossRef](#)] [[PubMed](#)]
48. Luo, S.; McNeill, M.; Myers, T.G.; Hohman, R.J.; Levine, R.L. Lon Protease Promotes Survival of Escherichia Coli During Anaerobic Glucose Starvation. *Arch. Microbiol.* **2008**, *189*, 181. [[CrossRef](#)]
49. He, L.; Luo, D.; Yang, F.; Li, C.; Zhang, X.; Deng, H.; Zhang, J.R. Multiple Domains of Bacterial and Human Lon Proteases Define Substrate Selectivity. *Emerg. Microbes Infect.* **2018**, *7*, 1–18. [[CrossRef](#)]
50. Stadtman, E.R.; Levine, R.L. Free Radical-Mediated Oxidation of Free Amino Acids and Amino Acid Residues in Proteins. *Amino Acids* **2003**, *25*, 207–218. [[CrossRef](#)]
51. Torres-Cabassa, A.; Gottesman, S.; Frederick, R.D.; Dolph, P.J.; Coplin, D.L. Control of Extracellular Polysaccharide Synthesis in Erwinia Stewartii and Escherichia Coli K-12: A Common Regulatory Function. *J. Bacteriol.* **1987**, *169*, 4525. [[CrossRef](#)]
52. Mukherjee, S.; Bree, A.C.; Liu, J.; Patrick, J.E.; Chien, P.; Kearns, D.B. Adaptor-Mediated Lon Proteolysis Restricts Bacillus Subtilis Hyperflagellation. *Proc. Natl. Acad. Sci. USA* **2015**, *112*, 250–255. [[CrossRef](#)]
53. Bissonnette, S.A.; Rivera-Rivera, I.; Sauer, R.T.; Baker, T.A. The IbpA and IbpB Small Heat-Shock Proteins Are Substrates of the AAA+ Lon Protease. *Mol. Microbiol.* **2010**, *75*, 1539. [[CrossRef](#)]
54. Shan, Y.; Gandt, A.B.; Rowe, S.E.; Deisinger, J.P.; Conlon, B.P.; Lewis, K. ATP-Dependent Persister Formation in Escherichia Coli. *mBio* **2017**, *8*, e02267-16. [[CrossRef](#)]
55. Ricci, V.; Blair, J.M.A.; Piddock, L.J.V. RamA, Which Controls Expression of the MDR Efflux Pump AcrAB-TolC, Is Regulated by the Lon Protease. *J. Antimicrob. Chemother.* **2014**, *69*, 643. [[CrossRef](#)] [[PubMed](#)]
56. Herbst, K.; Bujara, M.; Heroven, A.K.; Opitz, W.; Weichert, M.; Zimmermann, A.; Dersch, P. Intrinsic Thermal Sensing Controls Proteolysis of Yersinia Virulence Regulator RovA. *PLoS Pathog.* **2009**, *5*, 1000435. [[CrossRef](#)] [[PubMed](#)]
57. EmrK—Probable Multidrug Resistance Protein EmrK—Escherichia Coli (Strain K12) | UniProtKB | UniProt. Available online: <https://www.uniprot.org/uniprotkb/P52599/entry> (accessed on 7 November 2022).
58. YbhG—UPF0194 Membrane Protein YbhG—Escherichia Coli (Strain K12) | UniProtKB | UniProt. Available online: <https://www.uniprot.org/uniprotkb/P75777/entry> (accessed on 7 November 2022).
59. Moore, S.D.; Sauer, R.T. Revisiting the Mechanism of Macrolide-Antibiotic Resistance Mediated by Ribosomal Protein L22. *Proc. Natl. Acad. Sci. USA* **2008**, *105*, 18261–18266. [[CrossRef](#)] [[PubMed](#)]
60. Davydova, N.; Streltsov, V.; Wilce, M.; Liljas, A.; Garber, M. L22 Ribosomal Protein and Effect of Its Mutation on Ribosome Resistance to Erythromycin. *J. Mol. Biol.* **2002**, *322*, 635–644. [[CrossRef](#)] [[PubMed](#)]
61. Carlson, M.A.; Haddad, B.G.; Weis, A.J.; Blackwood, C.S.; Shelton, C.D.; Wuerth, M.E.; Walter, J.D.; Spiegel, P.C. Ribosomal Protein L7/L12 Is Required for GTPase Translation Factors EF-G, RF3 and IF2 to Bind in Their GTP State to 70S Ribosomes. *FEBS J.* **2017**, *284*, 1631. [[CrossRef](#)]
62. Starosta, A.L.; Lassak, J.; Jung, K.; Wilson, D.N. The Bacterial Translation Stress Response. *FEMS Microbiol. Rev.* **2014**, *38*, 1172. [[CrossRef](#)] [[PubMed](#)]
63. Chen, C.; Cui, X.; Beausang, J.F.; Zhang, H.; Farrell, I.; Cooperman, B.S.; Goldman, Y.E. Elongation Factor G Initiates Translocation through a Power Stroke. *Proc. Natl. Acad. Sci. USA* **2016**, *113*, 7515–7520. [[CrossRef](#)]
64. Divakaruni, A.V.; Baida, C.; White, C.L.; Gober, J.W. The Cell Shape Proteins MreB and MreC Control Cell Morphogenesis by Positioning Cell Wall Synthetic Complexes. *Mol. Microbiol.* **2007**, *66*, 174–188. [[CrossRef](#)] [[PubMed](#)]
65. Dik, D.A.; Marous, D.R.; Fisher, J.F.; Mobashery, S. Lytic Transglycosylases: Concinnity in Concision of the Bacterial Cell Wall. *Crit. Rev. Biochem. Mol. Biol.* **2017**, *52*, 503–542. [[CrossRef](#)]

66. Hung, W.C.; Jane, W.N.; Wong, H.C. Association of a D-Alanyl-D-Alanine Carboxypeptidase Gene with the Formation of Aberrantly Shaped Cells during the Induction of Viable but Nonculturable *Vibrio Parahaemolyticus*. *Appl. Environ. Microbiol.* **2013**, *79*, 7305–7312. [[CrossRef](#)] [[PubMed](#)]
67. Mueller, E.A.; Levin, P.A. Bacterial Cell Wall Quality Control during Environmental Stress. *mBio* **2020**, *11*, e02456-20. [[CrossRef](#)] [[PubMed](#)]
68. Szurmant, H.; Bu, L.; Brooks, C.L.; Hoch, J.A. An Essential Sensor Histidine Kinase Controlled by Transmembrane Helix Interactions with Its Auxiliary Proteins. *Proc. Natl. Acad. Sci. USA* **2008**, *105*, 5891–5896. [[CrossRef](#)] [[PubMed](#)]
69. Cheung, J.; Le-Khac, M.; Hendrickson, W.A. Crystal structure of a histidine kinase sensor domain with similarity to periplasmic binding proteins. *Proteins* **2009**, *77*, 235–241. [[CrossRef](#)] [[PubMed](#)]
70. Wang, H.W.; Chung, C.H.; Ma, T.Y.; Wong, H.C. Roles of Alkyl Hydroperoxide Reductase Subunit C (AhpC) in Viable but Nonculturable *Vibrio Parahaemolyticus*. *Appl. Environ. Microbiol.* **2013**, *79*, 3734–3743. [[CrossRef](#)]
71. Chen, L.; Xie, Q.W.; Nathan, C. Alkyl Hydroperoxide Reductase Subunit C (AhpC) Protects Bacterial and Human Cells against Reactive Nitrogen Intermediates. *Mol. Cell* **1998**, *1*, 795–805. [[CrossRef](#)]
72. Yuan, F.; Yin, S.; Xu, Y.; Xiang, L.; Wang, H.; Li, Z.; Fan, K.; Pan, G. The Richness and Diversity of Catalases in Bacteria. *Front. Microbiol.* **2021**, *12*, 485. [[CrossRef](#)]